Pramana – J. Phys. (2021) 95:120
https://doi.org/10.1007/s12043-021-02149-2

Steadily revolving flow of Sisko fluid along a stretchable boundary with non-linear radiation effects

TALAT RAFIQ and M MUSTAFA*

School of Natural Sciences (SNS), National University of Sciences and Technology (NUST), Islamabad 44000, Pakistan
*Corresponding author. E-mail: meraj_mm@hotmail.com

MS received 24 August 2020; revised 10 March 2021; accepted 12 March 2021

Abstract. The heat transfer effects in rotating flow above an extensible surface immersed in a non-Newtonian fluid obeying Sisko fluid model is considered in this article. The model is widely accepted for analysing flow behaviour of many industrial liquids including lubricating greases. Thermal transport existing in the non-linear radiative heat flux is investigated. Conservation equations are simplified using boundary layer approximations before these are reduced to locally similar differential equations through appropriate transformations. We adopted a highly convenient package bvp4c of MATLAB to find numerical results for both integer and non-integer values of flow behaviour index n. Solutions are analysed graphically for diverse range of controlling parameters. Akin to the earlier works, temperature curve exhibits an inflection point in the case of relatively large wall temperature. Furthermore, wall temperature gradient vanishes for increasing values of temperature ratio parameter. Graphical results demonstrate that stretching effect combined with Sisko fluid assumption can provide considerable improvement in the cooling process of the surface, which is certainly beneficial in some technological processes.

Keywords. Sisko model; rotating flows; non-linear radiative heat flux; stretchable surface; numerical method.

PACS Nos **47.10.−g; 47.10.A−; 47.10.ab**

1. Introduction

Heat transfer in non-Newtonian flows has been an attractive research topic for decades because of its bearing in real-life situations such as food, gas and chemical industries, civil and mechanical engineering, and in biomechanics to name just a few. Particularly, models of non-Newtonian fluids give rise to mathematical problems which are challenging compared with those concerning Navier–Stokes fluids. Power-law model, proposed by Ostwald-de-Waele, has received widespread acceptance because it provides the simplest possible representation of the shear thinning/thickening behaviour. Sisko [1] developed a simple model representing the flow of lubricating greases, using the available experimental data. His model was a generalisation of the usual power-law model. Existing literature confirms that relativity less research is conducted using power-law and Sisko models compared to their Newtonian counterpart. Cortell [2] considered fluid flow driven by an extensible surface lying in an incompressible MHD power-law fluid. He was able to develop local similarity solutions for diverse ranges of power-law index n. Akyildiz *et al* [3] analysed implicit differential equation associated with a steady flow of Sisko fluid. Fluid flow around a revolving cylinder in a power-law fluid was addressed by Panda and Chhabra [4]. Their numerical study was focussed towards estimating drag and lift coefficients for a wide range of power-law indices. Mekheimer *et al* [5] formulated reaction effects on the blood flow through anisotropically tapered artery with stenosis utilising the Sisko model. Malik *et al* [6] considered non-Fourier heat conduction approach to explore fluid flow along a non-linearly deforming sheet in a Sisko fluid. Later, Ahmed and Iqbal [7] deliberated heat transfer through Darcy–Brinkman porous media in annular sector filling power-law fluid. Zhuang *et al* [8] analysed double diffusive convection in porous medium saturating power-law fluid. Mahmood *et al* [9] addressed thermal transport in fluid flow due to non-linearly deforming surface in a Sisko fluid. Fluid flow in the vicinity of a stretchable hollow cylinder immersed in a Sisko fluid was studied by Hussain *et al* [10] using boundary layer approximations. Khan *et al* [11] examined non-linear radiation effects in

Published online: 18 July 2021

Sisko fluid flow using an analytical solution. Ibrahim and Seyoum [12] reported numerical results for Sisko fluid flow triggered by stretching surface in a rotating frame with nanoparticles.

The problems representing rotating flows along stationary or moving/rotating bodies have acquired importance in applied fluid mechanics, firstly because these exhibit similarity solution of the Navier–Stokes equations and secondly, such flows are predominant in chemical processes (chemical mixing chamber, spinning disk reactors and rheometers), industrial applications (turbines, electro-chemical and computer storage devices), geophysical applications (geothermal extraction, flows arising in geological formation owing to Earth's rotation, magma flow in Earth's mantle etc.) and oceanography. Wang [13] formulated fluid flow triggered by stretching of a horizontal surface by considering fluid rotation about the vertical axis. He was able to convert the full Navier–Stokes equations into a self-similar system comprising a parameter λ, which measures the importance of fluid rotation rate relative to the surface stretch rate. Wang's solution was based on a perturbation approximation valid for small values of λ. Later, Rajeswari and Nath [14] revisited Wang's work by considering time-dependent stretching rate of the bounding surface and obtained accurate solutions using finite difference scheme. Nazar *et al* [15] considered unsteady revolving flow induced by impulsive deformation of plane surface. They separately analysed the initial unsteady flow and steady-state situations. Kumari *et al* [16] investigated the steadily revolving flow of power-law fluid along an extensible surface utilising Keller-Box numerical procedure. Hayat *et al* [17] produced analytic approximations for MHD second-grade fluid flow past a porous shrinking surface. Javed *et al* [18] presented locally similar solutions for the rotating flow triggered by an exponentially deforming plate. Khan *et al* [19] carried out a numerical analysis for the rotating flow above a stretchable surface in a nanofluid considering single-phase nanofluid model approximation. Recent contributions towards this area include the works of Turkyilmazoglu [20], Sreelakshmi *et al* [21], Ahmad and Mustafa [22], Mustafa and Khan [23], Hamid *et al* [24] and Waini *et al* [25].

The motive of this research is to examine heat transfer process in the rotating flow of non-Newtonian fluid obeying Sisko model, over a deforming plane surface. Formulation is made in the rotating frame of reference. Unlike the existing research on the topic, Rosseland radiative heat flux expression (without linearisation) is invoked in the model development, resulting in the non-linear equation in temperature field. This makes the current analysis valid for both small and large temperature differences. Main interest here is to seek how rotational effects combined with the Sisko fluid assumption influence the resulting heat transfer rate and resisting wall shear. Computations are executed using a numerical method, which agrees well with the published data for power-law fluids. We also computed the admissible range of wall temperature ratio for which numerical solution is possible. Next section includes governing model obtained by using boundary layer approximations. Section 3 describes the numerical procedure that is to be executed in bvp4c package of MATLAB. Section 4 briefly explains the numerical results obtained. In §5, notable outcomes of this research are highlighted.

2. Problem formulation

We assume fluid motion along a stretchable radiative surface immersed in a rotating non-Newtonian fluid obeying Sisko model. This model explains shear-thinning/thickening features of the fluid. The elastic surface lies in the xy-plane while fluid occupies the semi-infinite region $z > 0$. Fluid rotation is considered about the z-axis with constant angular velocity ω. Furthermore, the surface stretches (expands) in the x-direction with linearly varying velocity $u_w = cx$, where $c > 0$ is a positive constant. The surface is assumed to be isothermal at temperature T_w, whereas T_∞ is termed ambient temperature. Sisko [1] proposed the following extra stress tensor:

$$\mathbf{S} = \left(a + b \left| \frac{\mathrm{tr}\left(\mathbf{A}_1^2\right)}{2} \right|^{\frac{n-1}{2}} \right) A_1, \tag{1}$$

where a and b are positive constants, $\mathbf{A}_1 = (\mathrm{grad}\ \mathbf{V}) + (\mathrm{grad}\ \mathbf{V})^T$ is the first Rivlin–Erickson tensor, $\mathbf{V}$ is the velocity vector. For $a = 0$, eq. (1) reduces to the well-known power-law model.

Accounting the assumptions outlined above together with boundary layer approximations, the conservation equations can be put in the following forms:

$$\frac{\partial u}{\partial x} + \frac{\partial w}{\partial z} = 0, \tag{2}$$

$$\rho\left(u\frac{\partial u}{\partial x} + w\frac{\partial u}{\partial z} - 2\omega v\right) = a\frac{\partial^2 u}{\partial z^2} + b\frac{\partial}{\partial z}\left\{\left[\left(\frac{\partial u}{\partial z}\right)^2 + \left(\frac{\partial v}{\partial z}\right)^2\right]^{\frac{n-1}{2}}\frac{\partial u}{\partial z}\right\}, \tag{3}$$

$$\rho\left(u\frac{\partial v}{\partial x} + w\frac{\partial v}{\partial z} + 2\omega u\right) = a\frac{\partial^2 v}{\partial z^2}$$

$$+b\frac{\partial}{\partial z}\left\{\left[\left(\frac{\partial u}{\partial z}\right)^2+\left(\frac{\partial v}{\partial z}\right)^2\right]^{\frac{n-1}{2}}\frac{\partial v}{\partial z}\right\}, \tag{4}$$

$$u\frac{\partial T}{\partial x}+w\frac{\partial T}{\partial z}=\frac{1}{\rho c_p}\left(\kappa\frac{\partial^2 T}{\partial z^2}-\frac{\partial q_r}{\partial z}\right), \tag{5}$$

where (u, v, w) denote velocities in the (x, y, z) directions respectively, κ represents thermal conductivity, c_p is the specific heat at constant pressure and $q_r = -(4\sigma^*/3k^*)\,\partial T^4/\partial z = -(16\sigma^*/3k^*)\,T^3\partial T^4/\partial z$ is the radiative heat flux [26], where σ^* and k^* are the Stefan–Boltzman constant and the mean absorption coefficient respectively.

The above equations are subjected to the following constraints:

$$\begin{aligned}&\text{at } z=0,\ u=cx,\ v=0,\ w=0,\ T=T_w,\\&\text{as } z\to\infty,\ u\to 0,\ v\to 0,\ T\to T_\infty.\end{aligned} \tag{6}$$

2.1 *Locally similar system*

Following Kumari *et al* [16], we proceed by introducing the transformations:

$$\begin{aligned}&u=cxF'(\zeta),\quad v=cxG(\zeta),\\&w=-\frac{2n}{n+1}\left(\frac{\rho c^{1-2n}}{b}\right)^{\frac{-1}{1+n}}x^{\frac{n-1}{n+1}}F(\zeta),\\&T=T_\infty+(T_w-T_\infty)\theta(\zeta),\\&\zeta=\left(\frac{\rho c^{2-n}}{b}\right)^{\frac{1}{n+1}}x^{\frac{1-n}{1+n}}z.\end{aligned} \tag{7}$$

Note that continuity equation (2) is fulfilled by variables (7), while eqs (3)–(5) convert to the following ODEs:

$$\Lambda F'''+\left\{\left(F''^2+G'^2\right)^{\frac{n-1}{2}}F''\right\}'+\frac{2n}{n+1}FF''+2\lambda G-F'^2=0 \tag{8}$$

$$\Lambda G''+\left\{\left(F''^2+G'^2\right)^{\frac{n-1}{2}}F''\right\}'+\frac{2n}{n+1}FG'-F'G-2\lambda F'=0 \tag{9}$$

$$\left[\left\{1+Rd\left(1+(\theta_w-1)\theta\right)^3\right\}\theta'\right]'+\frac{2n}{n+1}\mathrm{Pr}\theta' F=0 \tag{10}$$

with the boundary conditions

$$\begin{aligned}&F(0)=0,\ F'(0)=1,\ G(0)=0,\ \theta(0)=1,\\&F'\to 0,\ G\to 0,\ \theta\to 0\quad \text{as } \zeta\to\infty,\end{aligned} \tag{11}$$

where $\lambda=\omega/c$ is the rotation-strength parameter, $\Lambda = R_{e_x}^{2/n+1}/R_{e_a}$ is the material parameter of the Sisko fluid in which $R_{e_a}=\rho c x^2/a$ and $R_{e_x}=\rho x^n\,(cx)^{2-n}/b$, $\theta_w = T_w/T_\infty$ is the temperature ratio parameter, $Rd = 16\sigma^* T_\infty^3/3\kappa k^*$ is the radiation parameter (see [27–30]) and $\mathrm{Pr} = (cx^2 R_{e_x}^{-2/n+1})/\left(\kappa/\rho c_p\right)$ is termed as generalised Prandtl number.

2.2 *Skin friction coefficients*

We define the skin friction coefficients along the x- and y-directions as follows:

$$C_{fx}=\frac{\tau_{xz}|_{z=0}}{\rho(cx)^2},\quad C_{fy}=\frac{\tau_{yz}|_{z=0}}{\rho(cx)^2}, \tag{12}$$

where τ_{xz} and τ_{yz} are obtained from eq. (1) as follows:

$$\tau_{xz}=a\frac{\partial u}{\partial z}+b\left\{\left(\frac{\partial u}{\partial z}\right)^2+\left(\frac{\partial v}{\partial z}\right)^2\right\}^{\frac{n-1}{2}}\frac{\partial u}{\partial z}, \tag{13}$$

$$\tau_{yz}=a\frac{\partial v}{\partial z}+b\left\{\left(\frac{\partial u}{\partial z}\right)^2+\left(\frac{\partial v}{\partial z}\right)^2\right\}^{\frac{n-1}{2}}\frac{\partial v}{\partial z}. \tag{14}$$

Substituting eqs (13) and (14) in eq. (12) and then applying the transformations (7), we retrieve the following:

$$\begin{aligned}C_{fx}Re_x^{1/n+1}&=\left\{\Lambda+\left(F''(0)^2+G'(0)^2\right)^{\frac{n-1}{2}}\right\}F''(0)\Big\}\\C_{fy}Re_x^{1/n+1}&=\left[\Lambda+\left(F''(0)^2+G'(0)^2\right)^{\frac{n-1}{2}}\right\}G''(0)\Big]\end{aligned} \tag{15}$$

2.3 *Local Nusselt number*

Heat transfer from the elastic surface can be evaluated by the local Nusselt number Nu_x, defined as follows:

$$Nu_x=\frac{xq_w}{\kappa\,(T_w-T_\infty)}, \tag{16}$$

in which $q_w = -\kappa\,(\partial T/\partial z)_{z=0}+(q_r)_{z=0}$ specifies wall heat flux from the boundary. Substituting (7) into (16) we get

$$Nu_x\,(Re_x)^{-1/n+1}=-\left(1+Rd\theta_w^3\right)\theta'(0). \tag{17}$$

Equation (17) clearly suggests that heat transfer rate is proportional to θ_w, which arises due to non-linear radiative flux consideration.

3. Numerical procedure

The solution of two-point boundary-value problem comprising eqs (8)–(10) with conditions (11) is sought by the reliable package bvp4c of MATLAB. Numerical method appears suitable for values of flow behaviour index (n) in the range $0 \leqslant n \leqslant 2$ which encompasses both pseudoplastic and dilatant-type fluids. To begin with, we convert the governing problem into a system of first-order equations by substituting

$$y_1 = F,\ y_2 = F',\ y_3 = F'',\ y_4 = G,\ y_5 = G',$$
$$y_6 = \theta \text{ and } y_7 = \theta'. \tag{18}$$

The corresponding first-order system is given as follows:

$$y_1' = y_2, \tag{19}$$
$$y_2' = y_3, \tag{20}$$
$$y_3' = \frac{My_5\left(-y_2y_3y_4 - 2\lambda y_2y_3 - 2\lambda y_4y_5 + y_5y_2^2\right) - N\left(\frac{2n}{n+1}y_1y_3 + 2\lambda y_4 - y_2^2\right)}{N\left(\Lambda + n\left(y_3^2 + y_5^2\right)^{(n-1)/2}\right)}, \tag{21}$$
$$y_4' = y_5, \tag{22}$$
$$y_5' = \frac{My_3\left(-y_2^2y_5 + 2\lambda y_4y_5 + y_2y_3y_4 + 2\lambda y_2y_3\right) - N\left(\frac{2n}{n+1}y_1y_5 - y_2y_4 - 2\lambda y_2\right)}{N\left(\Lambda + n\left(y_3^2 + y_5^2\right)^{(n-1)/2}\right)}, \tag{23}$$
$$y_6' = y_7, \tag{24}$$
$$y_7' = \frac{-\frac{2n}{n+1}Pry_1y_7 - 3Rdy_7^2\left(\theta_w - 1\right)\left(1 + \left(\theta_w - 1\right)y_6\right)^2}{1 + Rd\left(1 + \left(\theta_w - 1\right)y_6\right)^3}, \tag{25}$$

where

$$M = \left((n-1)\left(y_3^2 + y_5^2\right)^{(n-3)/2}\right)$$

and

$$N = \left(\Lambda + \left(y_3^2 + y_5^2\right)^{(n-1)/2}\right).$$

Equations (21), (23) and (25) subject to boundary conditions (11) are written in the bvp4c code. The problem is initially solved in a smaller domain $[0, L]$ and then value of L is increased until the initial slopes $F''(0)$, $G'(0)$ and $\theta'(0)$ become independent of the chosen L.

4. Results and discussion

To ensure that MATLAB code is working fine, results of $F''(0)$ and $G'(0)$ are compared with those reported by Kumari *et al* [16]. Table 1 shows that all the results are similar to that of [16] for all values of λ. In table 2 we include the skin friction coefficient and Nusselt number data evaluated by varying fluid rotation parameter λ, the material parameter of Sisko fluid Λ and power-law index n. It is predicted that by increasing the parameter Λ, the normalised skin friction factor should be lowered. The highest and lowest values of heat transfer rate occur, for $\lambda = 0$ and $\lambda = 2$ respectively when $\Lambda = 1$. Table 3 elucidates how local Nusselt number is affected by the parameters appearing in the energy equation. This table shows that higher heat transfer rate can be achieved by imposing higher temperature difference. Furthermore, strength of radiative flux also boosts heat transfer from the solid surface.

Figures 1a–1d show variations in the velocity and the temperature curves by varying rotation-strength parameter λ in Newtonian fluid case ($n = 1$). In rotating frame of reference, the velocity curves exhibit damped oscillations in ζ. The amplitude of such oscillations is higher when rotation rate is large compared to the surface stretch rate. In non-rotating frame ($\lambda = 0$), velocity curves are monotonically decreasing functions of ζ. Note that G-profile representing $v-$velocity component is negative signalling that counterclockwise fluid rotation induces fluid flow in the negative y-direction only. The influence of λ is to clearly suppress the hydrodynamic boundary layer. In contrast, an expansion in thermal penetration depth is seen for increasing values of λ. Physically, the vertical (or downward) fluid motion slows down as λ increases. This in turn reduces the intensity of cold fluid (at the far-field) towards the hot surface, which thereby thickens the thermal boundary layer.

The results of figures 1a–1d are re-obtained by considering non-Newtonian effects with $\Lambda = 1$ in figures 2a–2d. Note that the values $n = 0.5$ and 1.5 are valid for pseudoplastic and dilatant fluids respectively. In pseudoplastic fluids, the momentum penetration depth is shorter than that in the dilatant fluids. The remarkable effect of rheology is the thinning of hydrodynamic

Table 1. Numerical results of $F''(0)$ and $G'(0)$ in Newtonian fluid case ($n = 1$) with Pr = 5.

λ	Kumari *et al* [16]		Present result	
	$F''(0)$	$G'(0)$	$F''(0)$	$G'(0)$
0.0	−1.0000	0.0000	−0.999999	−0.000001
0.5	−1.13838	−0.51275	−1.138381	−0.512760
1.0	−1.32503	−0.83709	−1.325029	−0.837098
2.0	−1.65235	−1.28724	−1.652352	−1.287259

boundary layer upon increasing n. Also, variations in temperature curves appear to be prominent in pseudoplastic fluids when compared with dilatant fluids.

To forecast the role of material parameter Λ on the flow problem, we have presented figures 3a–3d. Appreciably, considerable influence of parameter Λ on the solution profiles is witnessed. By increasing Λ, we notice a reduction in the amplitude of oscillations in the velocity profiles. Fluid flow in the x-direction induced by the stretching surface accelerates as Λ increases. This results in enhanced vertical flow towards the surface which in turn reduces thermal boundary layer thickness. Figure 3d shows that fluid flow in the y-direction, generated by rotational effects, also increase for increasing values of Λ.

Figures 4a–4c elucidate variations in temperature profile by changing Prandtl number Pr, radiation parameter Rd and temperature ratio parameter θ_w for both pseudoplastic ($n = 0.5$) and dilatant ($n = 1.5$) fluids. Prandtl number Pr shows the importance of momentum diffusivity relative to the thermal diffusion. Hence, thermal convection becomes stronger than the thermal diffusion as Pr increases. This provides higher heat transfer per unit area of the surface resulting in thinner thermal boundary layer. The influence of rheology is such that temperature falls within the boundary layer for increasing values of n. In the presence of θ_w, temperature profile is concave down near the boundary and concave up far from it signalling the existence of inflection point, details of which are already explained in [28]. Figure 4d is prepared to determine the permissible range of parameters for which numerical solution is possible. For example, when $Rd = 1$, the bvp4c code returns numerical results in the range $1 \leqslant \theta_w \leqslant 5$. This range shrinks/expands as we increase/decrease the value of Rd.

Table 3. Effects of parameters Rd, θ_w and Pr on numerical results of local Nusselt number with $\lambda = n = 0.5$ and $\Lambda = 1$.

Rd	θ_w	Pr	$Nu_x\,(Re_x)^{-1/n+1}$
0.1	1.5	5	1.400220
1			2.091620
3			2.760320
5			3.047540
7			3.185493
1	1.1		1.767836
	1.5		2.091620
	2		2.528886
	3		3.221252
	4		3.424174
	1.5	0.7	0.454753
		1	0.628004
		2	1.107958
		5	2.091620
		7	2.582401
		5	2.091620

Table 2. Numerical results of $F''(0)$, $G'(0)$, skin friction coefficients and local Nusselt number for non-Newtonian fluid ($n \neq 1$) with Pr = 5, $Rd = 1$ and $\theta_w = 1.5$.

λ	Λ	n	$F''(0)$	$G'(0)$	$C_{fx}Re_x^{1/n+1}$	$C_{fy}Re_x^{1/n+1}$	$Nu_x\,(Re_x)^{-1/n+1}$
0	1	0.5	−0.687490	0.000000	−1.516640	0.000000	2.239523
0.5			−0.830669	−0.370609	−1.7016641	−0.759199	2.091620
1			−1.004374	−0.611604	−1.930572	−1.175604	1.898179
2			−1.304253	−0.965814	−2.328048	−1.723946	1.541493
0		1.5	−0.736968	0.000000	−1.369632	0.000000	3.047945
0.5			−0.802599	−0.354949	−1.554469	−0.687462	2.961248
1			−0.901109	−0.575284	−1.832825	−1.170110	2.821626
2			−1.075373	−0.863060	−2.338135	−1.876513	2.549826
0.5	0.5	0.5	−1.014518	−0.442055	−1.471656	−0.641243	1.981971
	1.5		−0.723208	−0.327164	−1.896552	−0.857959	2.161596
	3		−0.553863	−0.255908	−2.370667	−1.095346	2.278033
	0.5	1.5	−0.901076	−0.402508	−1.345688	−0.601115	2.862462
	1.5		−0.728697	−0.320349	−1.743184	−0.766335	3.029438
	3		−0.586133	−0.255484	−2.227082	−0.970743	3.150355

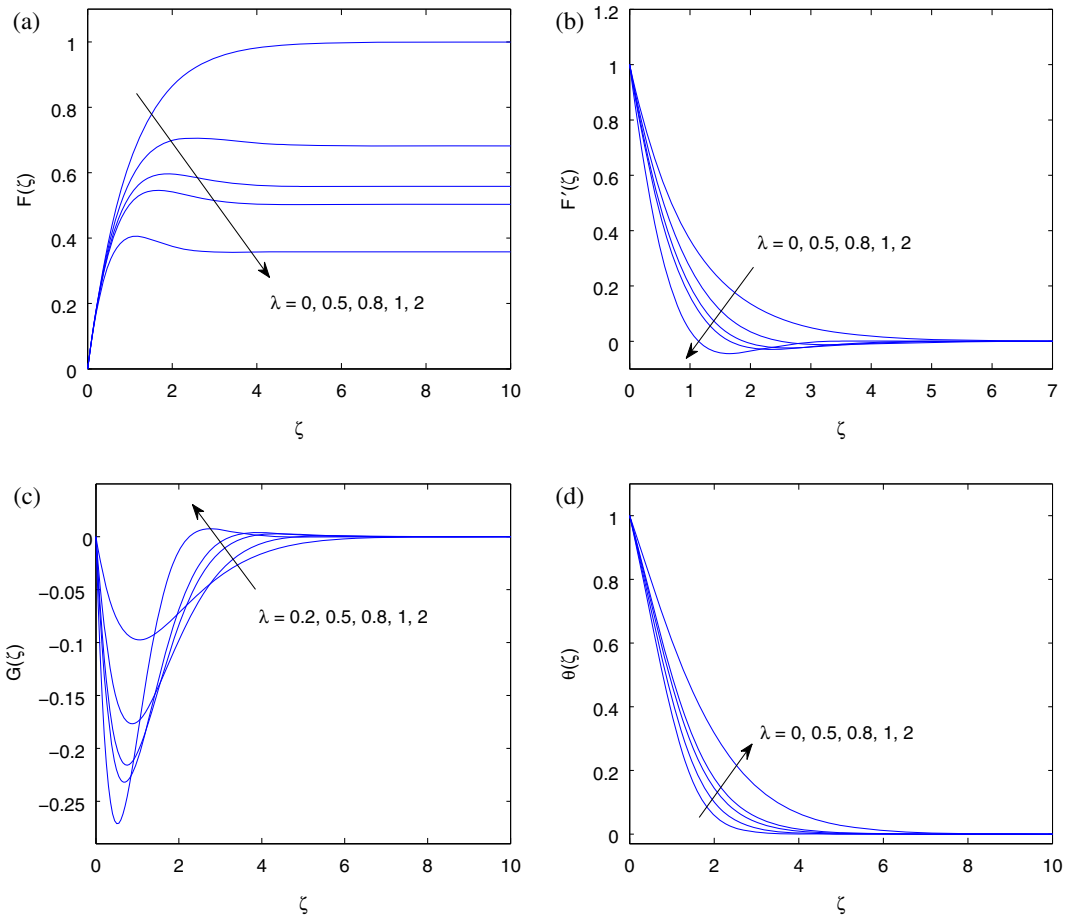

Figure 1. Velocity profiles (F, F', G) and temperature curve for various values of rotation strength parameter λ in the case of Newtonian fluid with Pr $= 5$, $Rd = 1$ and $\theta_w = 1.5$.

Figures 5a and 5b present the profiles of temperature gradient θ' for different values of θ_w and position of inflection point respectively for some specific parameter values. Figure 5a indicates that location of inflection point shifts away from the wall when θ_w increases. Figures 6a and 6b show the graphs of skin friction coefficients vs. λ by changing the material fluid parameter Λ. Rotational effect naturally contributes to the overall wall drag coefficient. Skin friction coefficient is directly proportional to the parameter n. Equation (1) apparently shows that fluid apparent viscosity is proportional to n. Increasing n therefore corresponds to a higher apparent viscosity which in turn gives higher skin friction coefficients.

Graphs of local Nusselt number vs. parameter λ are presented for different values of Λ and Pr in figures 7a and 7b. In rotating frame of reference, heat transfer rate is drastically lowered compared to the same in non-rotating frame. Intriguingly, power-law index n can remarkably improve the heat transfer rate. Moreover, Nusselt number becomes zero for vanishing Prandtl number Pr.

5. Concluding remarks

Steadily rotating flow along a stretchable (elastic) surface in the Sisko fluid is examined numerically. Equations of fluid motion and energy transfer are transformed into a locally similar system which is dealt numerically. Range of θ_w for which the desired tolerance criterion of numerical results is achievable is obtained. Main findings of this research are summarised as follows:

- Function $g(\eta)$ is negative illustrating that counterclockwise rotation induces fluid flow in the negative y-direction.
- Velocity curves exhibit damped oscillations in similarity variable η, which is attributed to the fluid rotation above the vertical axis. The envelope of oscillations suppresses for increasing values of material fluid parameter Λ.
- Effects of flow behaviour index on solutions are comparatively prominent in pseudoplastic fluids.
- Inclusion of radiative heat flux gives rise to a nonlinear energy equation in temperature comprising

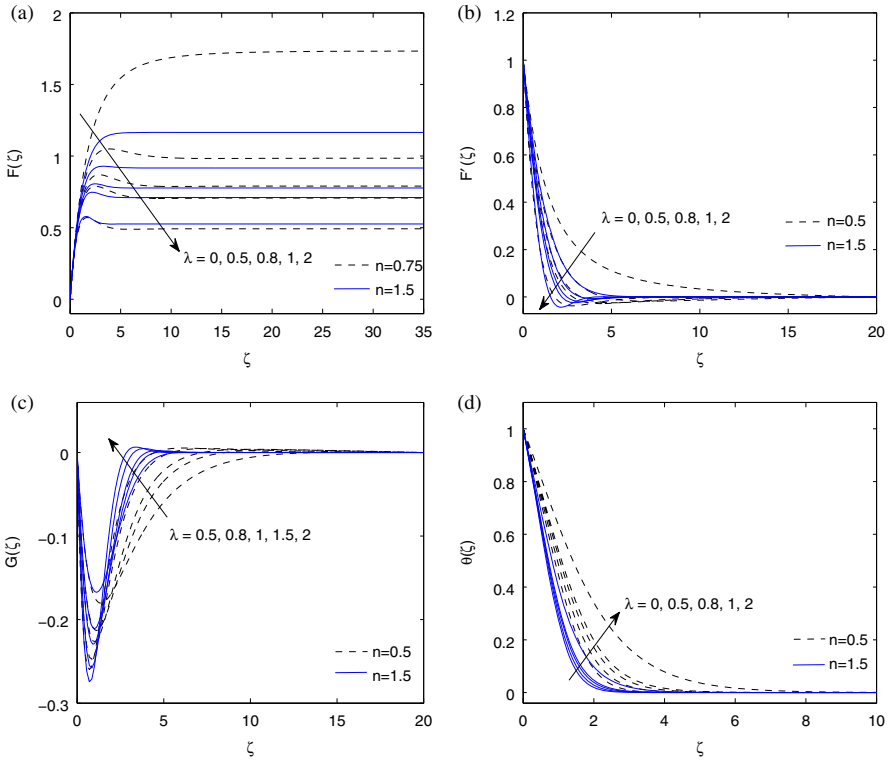

Figure 2. Velocity profiles $\left(F, F', G\right)$ and temperature (θ) for various values of rotation strength parameter λ when $\mathrm{Pr} = 5$, $Rd = 1, \theta_w = 1.5$ and $\Lambda = 1$.

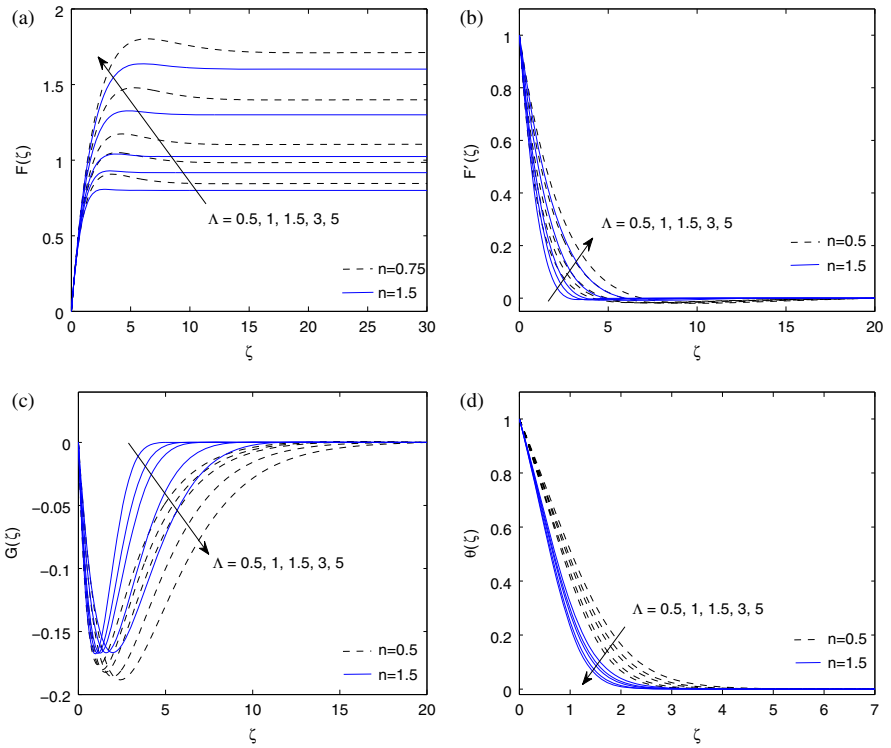

Figure 3. Velocity profiles $\left(F, F', G\right)$ and temperature (θ) for various values of Λ when $\mathrm{Pr} = 5$, $Rd = 1, \theta_w = 1.5$ and $\lambda = 0.5$.

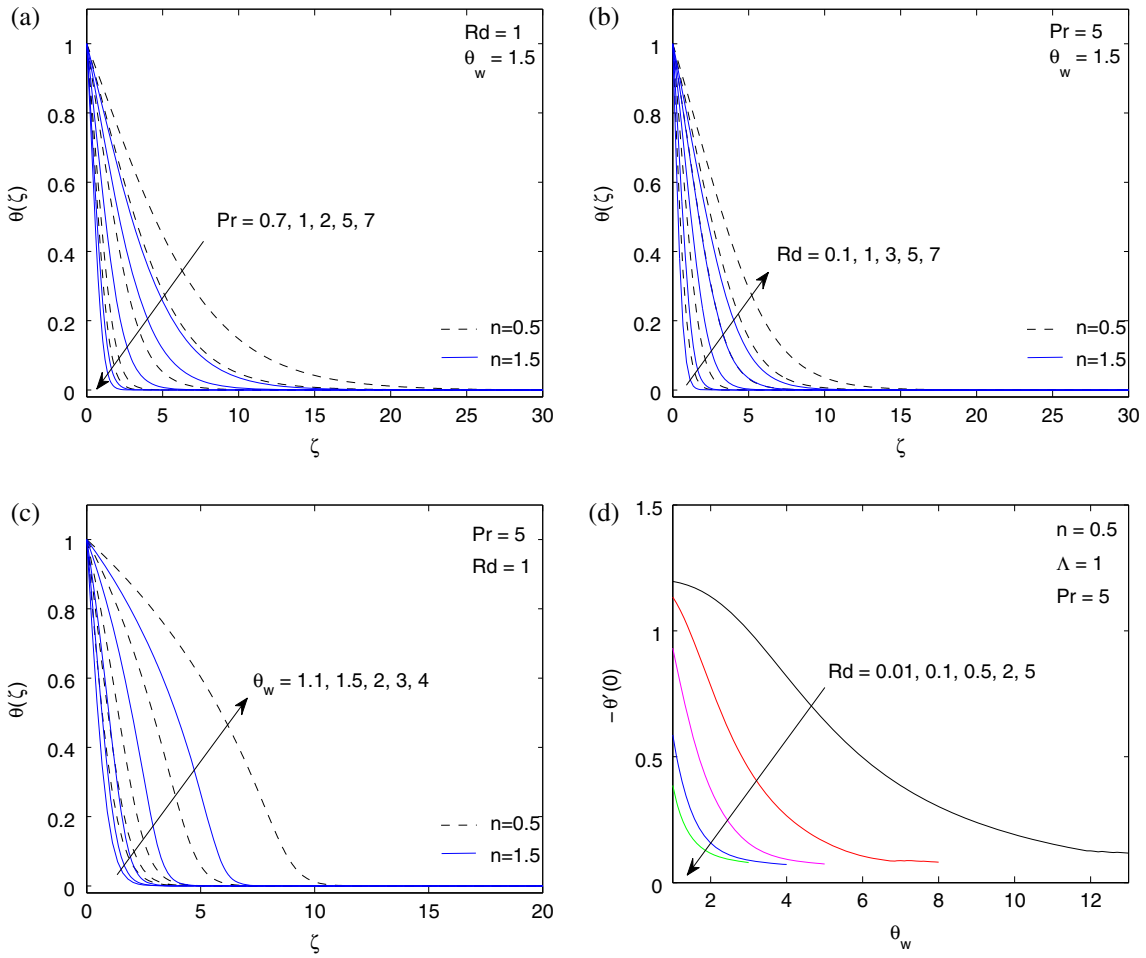

Figure 4. (**a**)–(**c**) Temperature profiles for various value of Pr, Rd and θ_w when $\lambda = 0.5$ and $\Lambda = 1.5$ and (**d**) admissible range of θ_w for numerical solution of eq. (10) for different values of Rd.

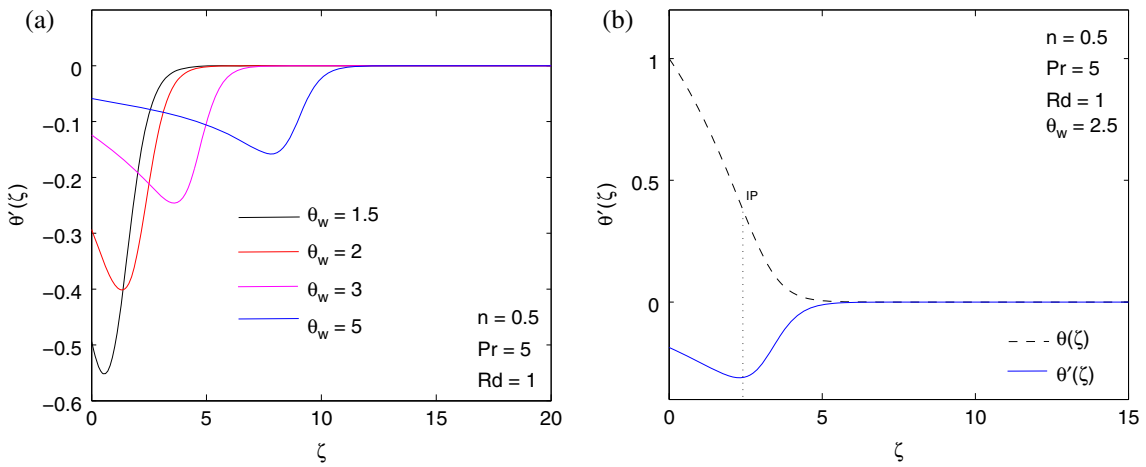

Figure 5. (**a**) Profiles of temperature gradient θ' for various values of θ_w and (**b**) position of inflection point when $\lambda = 0.5$ and $\Lambda = 1.5$.

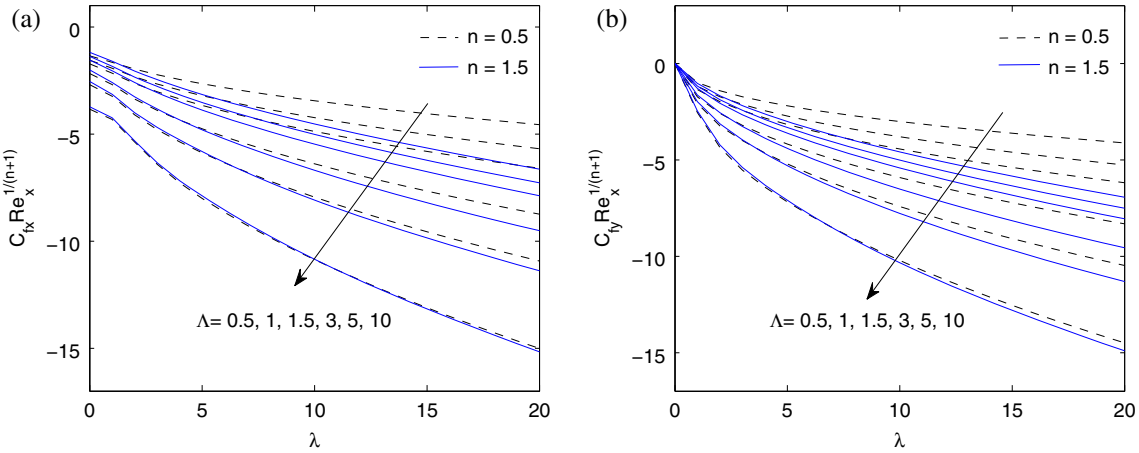

Figure 6. Skin friction coefficient vs. λ for different values of Λ in the x- and y-directions when Pr = 5.

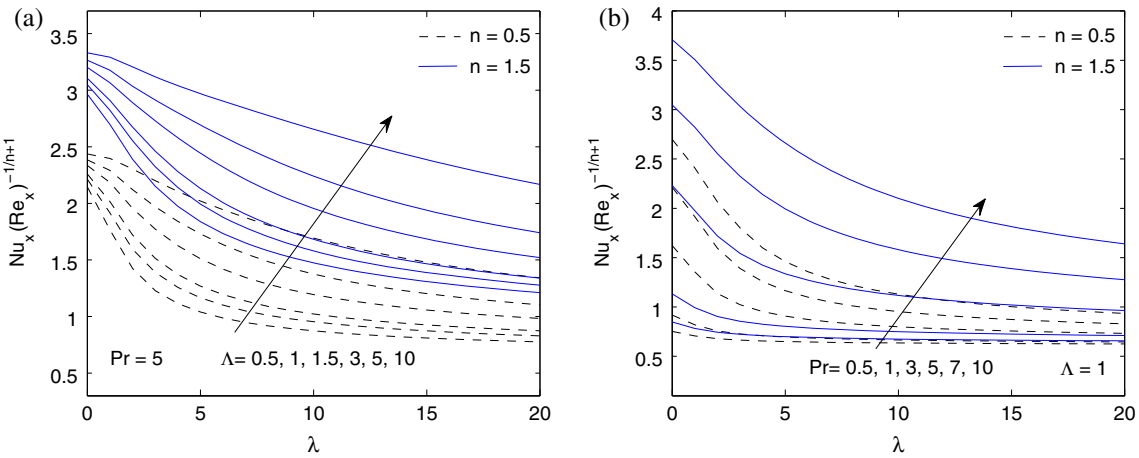

Figure 7. Profile of Nusselt number vs. λ for different values of Λ and Pr.

three parameters, namely the Prandtl number, the radiation parameter and the temperature ratio parameter.

- Akin to the past papers, temperature profile contains an inflection point, location of which shifts away from the wall as temperature difference enlarges.
- Drag experienced at the boundary elevates when either the flow behaviour index n or the rotation-strength parameter λ becomes large.
- Heat transfer from the boundary has inverse relationship with λ. Moreover, far field vertical velocity $F(\infty)$, measuring volumetric flow rate, increases when either λ or n increases.
- For a particular value of Rd, wall temperature gradient θ'' decays for increasing values of θ_w.

References

[1] A W Sisko, *Ind. Eng. Chem.* **50**, 1789 (1958)
[2] R Cortell, *Appl. Math. Comput.* **168**, 557 (2005)
[3] F T Akyildiz, K Vajravelu, R N Mohapatra, E Sweet and R A Van Gorder, *Appl. Math. Comput.* **210**, 189 (2009)
[4] S K Panda and R P Chhabra, *J. Non-Newtonian Fluid Mech.* **165**, 1442 (2010)
[5] Kh S Mekheimer and M A El Kot, *Appl. Math. Model.* **36**, 5393 (2012)
[6] R Malik, M Khan and M Mushtaq, *J. Mol. Liq.* **222**, 430 (2016)
[7] F Ahmed and M Iqbal, *Int. J. Mech. Sci.* **130**, 508 (2017)
[8] Y J Zhuang, H Z Yu and Q Y Zhu, *Int. J. Heat Mass Transf.* **115**, 670 (2017)

[9] T Mahmood, Z Iqbal, J Ahmed, A Shahzad and M Khan, *Res. Phys.* **7**, 2458 (2017)
[10] A Hussain, M Y Malik, T Salahuddin, S Bilal and M Awais, *J. Mol. Liq.* **231**, 341 (2017)
[11] M I Khan, S Qayyum, T Hayat, A Alsaedi and M I Khan, *J. Mol. Liq.* **257**, 155 (2018)
[12] W Ibrahim and J Seyoum, *J. Nanofluids* **8**, 1412 (2019)
[13] C Y Wang, *ZAMP* **39**, 177 (1988)
[14] V Rajeswari and G Nath, *Int. J. Eng. Sci.* **30**, 747 (1992)
[15] R Nazar, N Amin and I Pop, *Mech. Res. Commun.* **31**, 121 (2004)
[16] M Kumari, T Grosan and I Pop, *Tech. Mech.* **1**, 11 (2006)
[17] T Hayat, T Javed and M Sajid, *Phys. Lett. A* **372**, 3264 (2008)
[18] T Javed, Z Abbas, M Sajid and N Ali, *Int. J. Numer. Meth. Heat Fluid Flow* **21**, 903 (2011)
[19] J A Khan, M Mustafa and A Mushtaq, *Int. J. Heat Mass Transf.* **94**, 49 (2016)
[20] M Turkyilmazoglu, *Int. J. Mech. Sci.* **90**, 246 (2015)
[21] K Sreelakshmi, V Nagendramma and Sarojamma, *Proc. Eng.* **127**, 678 (2015)
[22] R Ahmad and M Mustafa, *J. Mol. Liq.* **220**, 635 (2016)
[23] M Mustafa and J A Khan, *J. Mol. Liq.* **234**, 287 (2017)
[24] M Hamid, M Usman, T Zubair, R Ul Haq and W Wang, *Int. J. Heat Mass Transf.* **124**, 706 (2018)
[25] I Waini, A Ishak and I Pop, *Int. J. Heat Mass Transf.* **136**, 288 (2019)
[26] S Rosseland, *Astrophysik and atom-theorestische-grundlagen* (Springer, Berlin, 1931)
[27] M Mustafa, R Ahmad, T Hayat and A Alsaedi, *Neural Comput. Appl.* **29**, 493 (2018)
[28] G Ibáñez, A López, I López, J Pantoja, J Moreira and O Lastres, *J. Therm. Anal. Calorim.* **135**, 3401 (2018)
[29] Z Abdelmalek, I Khan, M W A Khan, K Rehman and E S M Sherif, *J. Mater. Res. Tech.* **9**, 11035 (2020)
[30] M Khan, A Hafeez and J Ahmed, *Physica A*, https://doi.org/10.1016/j.physa.2019.124085 (2020)